Experimental Study on the Effect of Secondary Vortices at the Trailing Edge on Motion-Induced Vortex Vibration

Kazutoshi Matsuda[1*], Kusuo Kato[1], Nade Cao[1] and Ryoya Higashimura[1]

[1] Department of Civil Engineering and Architecture, Kyushu Institute of Technology
1-1 Sensui-cho, Tobata-ku, Kitakyushu, Fukuoka 804-8550, (Japan)
matsuda@civil.kyutech.ac.jp ; kato@civil.kyutech.ac.jp
sounatoku@gmail.com ; o105061r@mail.kyutech.jp

Abstract According to the results of conventional wind tunnel tests on rectangular cross sections with side ratios of *B/D*=2–8 (*B*: along-wind length (m), *D*: cross-wind length (m)), motion-induced vortex vibration was confirmed. The generation of motion-induced vortex vibration is considered to be caused by the unification of separated vortices from the leading edge and secondary vortices at the trailing edge. Spring-supported tests and smoke flow visualization tests for *B/D*=0.62, 0.75, 1.0, 1.18 and 1.50 were conducted in a wind tunnel at Kyushu Institute of Technology. As a result, it was considered that the secondary vortices at the trailing edge are not always essential for the generation of the motion-induced vortex vibration in heaving motion of each cross section. In this study, smoke flow visualizations were performed for side ratios of *B/D*=2.0, 4.0, 6.0 in order to elucidate the role of secondary vortices at the trailing edge in motion-induced vortex vibration in heaving motion. Spring-supported tests were also carried out in order to obtain the response characteristics of the models.

Keywords: motion-induced vortex vibration · smoke flow visualizations · spring-supported tests · rectangular cross sections · side ratios

1 Introduction

According to Shiraishi and Matsumoto (1983), the vortices separated from rectangular cross sections in wind tunnel tests are broadly classified into Kármán vortices and motion-induced vortices (vortices separated from the leading edge). Kármán vortices are accompanied by interference of the two separated shear layers at both the top and bottom surfaces of the structures. Motion-induced vortices are shed separately from the leading edges of the top and bottom surfaces, because the separated shear layers at the top and bottom surfaces are excited alternately due to the vibration of the rectangular cross section. The vibration caused by the latter vortices was found in past wind tunnel tests by Novak (1971) and Otsuki et al. (1971). The vibration is known as either

motion-induced vortex vibration (Shiraishi and Matsumoto (1983), Komatsu and Kobayashi (1980)) or impinging-shear-layer instability (Rockwell and Naudascher (1978), Nakamura et al. (1991), Ohya et al. (1992), Naudascher and Wang (1993)). The onset wind speed of this vibration depends on the side ratio of the rectangular cross section, and this relation has been schematically clarified by Shiraishi and Matsumoto (1983), Naudascher and Wang (1993).The generation of motion-induced vortex vibration is considered to be caused by the unification of separated vortices from the leading edge and secondary vortices at the trailing edge. Motion-induced vortex vibration was confirmed by conventional wind tunnel tests on rectangular cross sections with side ratios of B/D=2–8. However, in order to clarify the relation between the generation of motion-induced vortex in heaving motion and lower side ratios B/D, a visualization test for the smoke flows around the cross section was performed by providing a forced heaving oscillation on models of the rectangular cross sections of B/D=0.62, 0.75, 1.0, 1.18 and 1.50 by Matsuda et al. (2016) and Matsuda et al. (2017). As a result, it was considered that the secondary vortices at the trailing edge are not always essential for the generation of the motion-induced vortex vibration in heaving motion of each cross section.

The purpose of this study is to find out the role of the secondary vortex at trailing edge in heaving motion-induced vortex vibration of rectangular cross sections with side ratios of B/D=2.0, 4.0 and 6.0 by carried out smoke flow visualizations and spring-supported tests. Moreover, based on the results, this research aimed to verify whether or not the secondary vortices at the trailing edge are essential for the generation of motion-induced vortex vibration in heaving motion.

2 Experimental Setup

Smoke flow visualizations around the model during oscillating condition were conducted in a small-sized wind tunnel (0.4 m high×0.4 m wide×2.0 m long) at Kyushu Institute of Technology. Figs. 1 and 2 show the schematic illustration of experimental setup for smoke flow visualization and the forced oscillation system, respectively. It was presumed that wind speeds of V=0.6–1.0 m/s in the wind tunnel were good for visualization, so eventually V=0.8 m/s was selected as the onset wind speeds of motion-induced vortex vibration. Accordingly, the experimental Reynolds number was $Re=VD/\nu=1.1\times10^3$, where V: wind speed (m/s), D: cross-wind length (m), ν: kinematic viscosity (m^2/s). For the forced-oscillating amplitude η, the non-dimensional double amplitudes were set as $2\eta/D$=0.02-0.20 (every 0.01 intervals). Because the onset reduced wind speeds of motion-induced vortex vibration and Kármán vortex-induced vibration come close to each other on the cross section at roughly B/D = 2.8-6.0, according to Matsumoto et al. (1993a), smoke flow visualizations were conducted using a splitter plate (hereinafter referred as "S.P.") installed at the downstream side of the rectangular cross section model with the gap length g for the purpose of weakening

the Kármán vortex, as shown in Fig. 3. Table 1shows the experimental conditions for the smoke flow visualization tests. Spring-supported tests were also performed in order to get the response characteristics of the models. Table 2 shows the experimental conditions for the spring-supported tests. Laser displacement detectors were used for measuring an amplitude of the models. The spring-supported tests were conducted in a closed circuit wind tunnel (cross section: 1.8 m high×0.9 m wide) at Kyushu Institute of Technology. All wind tunnel tests were carried out in a smooth flow.

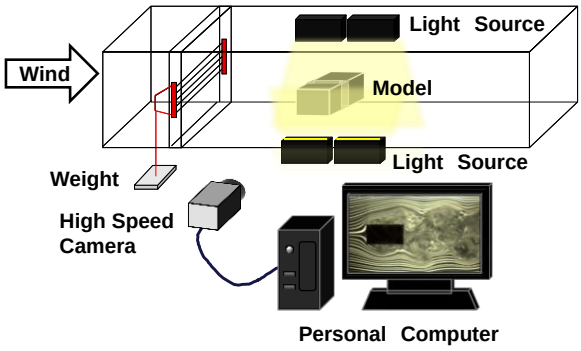

Fig. 1 Schematic illustration of experimental setup for smoke flow visualization

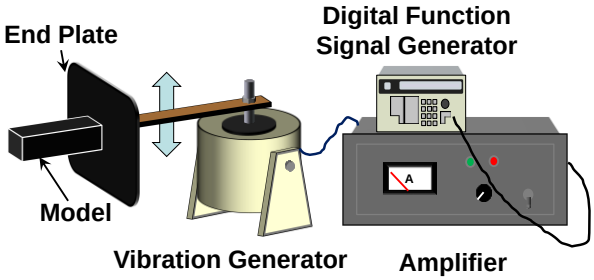

Fig. 2 Forced oscillation system for smoke flow visualization

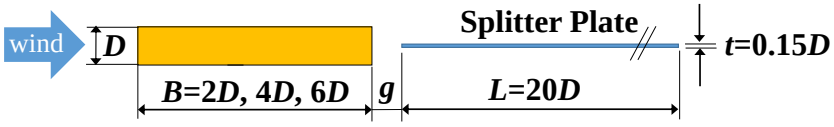

Fig. 3 Rectangular cross section model and splitter plate

Table 1 Experimental conditions for smoke flow visualization

B/D	*B* (m)	*D* (m)	Splitter Plate (S.P.)	Gap length between model and splitter plate *g*		Wind Speed *V* (m/s)	Reynoles Number *Re=VD/v*	Forced-oscillating Frequency *f* (Hz)	Reduced Wind Speed *Vr=V/fD*	Non-dimensional Forced-oscillating Double Amplitude *2η/D*
2	0.04	0.02	w/o	-	-	0.8	1.1×10^3	12.0	3.33 =1.67*B/D*	0.02-0.20
			w/o	-	-			7.34	5.45	0.20
			w/	0.20*D*	0.10*B*					
			w/	0.50*D*	0.25*B*					
4	0.08	0.02	w/o	-	-	0.8	1.1×10^3	12.0	3.33 =0.83*B/D*	0.02-0.18
			w/o	-	-			9.32	4.29	0.20
			w/	0.40*D*	0.10*B*					
			w/	1.25*D*	0.31*B*					
			w/o	-	-	0.8	1.1×10^3	6.00	6.67 =1.67*B/D*	0.02-0.34
			w/o	-	-			4.8	8.31	0.20
			w/	0.40*D*	0.10*B*					
			w/	1.25*D*	0.31*B*					
6	0.12	0.02	w/o	-	-	0.8	1.1×10^3	8.00	5.0 =0.83*B/D*	0.02-0.18
			w/o	-	-			7.43	5.38	0.20
			w/	0.60*D*	0.10*B*					
			w/	2.0*D*	0.33*B*					
			w/o	-	-			4.00	10.0 =1.67*B/D*	0.02-0.46

Table 2 Experimental conditions for spring-supported tests

B/D	*B* (m)	*D* (m)	Splitter Plate (S.P.)	Gap length between model and splitter plate *g*		Air Density *ρ* (kg/m^3)	Mass per Unit Length *m* (kg/m)	Structural Damping (Logarithmic Decrement) *δ*	Natural Frequency *f* (Hz)	*Sc =2m/ρD*^{2}
2	0.09	0.18	w/o	-	-	1.23	5.49	0.0043	5.22	4.7
			w/	0.20*D*	0.10*B*	1.24	5.35	0.0044	5.15	4.7
			w/	0.50*D*	0.25*B*	1.24	5.52	0.0048	5.20	5.2
4	0.09	0.36	w/o	-	-	1.25	3.82	0.0133	6.25	10.1
			w/	0.40*D*	0.10*B*	1.24	3.69	0.0135	6.20	9.9
			w/	1.25*D*	0.31*B*	1.23	3.85	0.0130	6.23	10.1
6	0.09	0.54	w/o	-	-	1.22	4.55	0.0156	5.73	14.4
			w/	0.60*D*	0.10*B*	1.23	4.44	0.0247	5.66	21.9
			w/	2.0*D*	0.33*B*	1.22	4.41	0.0162	5.67	14.4

3 Experimental Results and Discussion

3.1 B/D=2.0 Rectangular Cross Section

The results of the spring-supported test of B/D = 2.0 are shown in Fig. 4. The vortex-induced vibrations occurring at approximately Vr = 3 were confirmed. These vortex-induced vibrations are considered to be motion-induced vortex vibrations because they are occurring at around $V_{cr,n=1} = (1/n)1.67 \times B/D = 1.67 \times 2.0 = 3.33$ and there was no change in onset reduced wind speed due to S.P. being installed. The result shows that the nearer the S.P. was installed at the downstream side of the model, the lower the response amplitude became. Furthermore, the occurrence of Kármán vortex-induced vibration and galloping could be confirmed in the high wind speed region. Because the vibration occurred at the higher wind speed region in the two cases with S.P., rather than that without S.P., it was confirmed that Kármán vortices were weakened by S.P. The result of the experiment of flow visualization under the condition that reduced wind speed was Vr = 5.45, where the response amplitude becomes the maximum and the forced-oscillating heaving amplitude set as $2\eta/D$=0.2 was compared with the results of three cases where no S.P. was installed and cases where it was installed at g = 0.10B and g = 0.25B. The results are shown in Fig. 5. It was confirmed that the development of the integrated vortex of the separated vortex from the leading edge with the secondary vortex at the trailing edge was inhibited by the existence of S.P. It is considered that this is the reason why the response amplitude of motion-induced vortex vibration decreased when S.P. was installed.

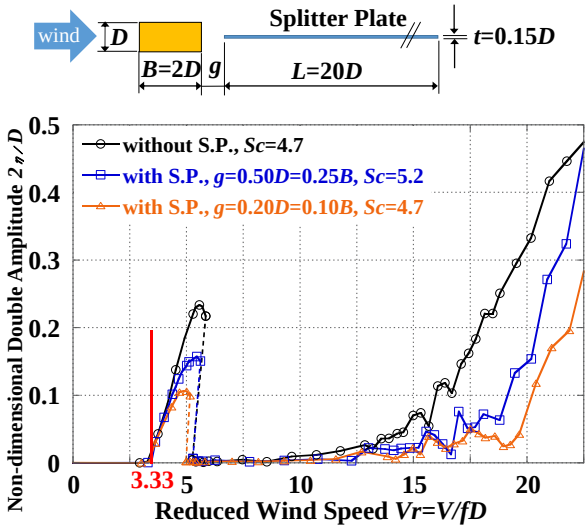

Fig. 4 Spring-supported test result of B/D=2.0

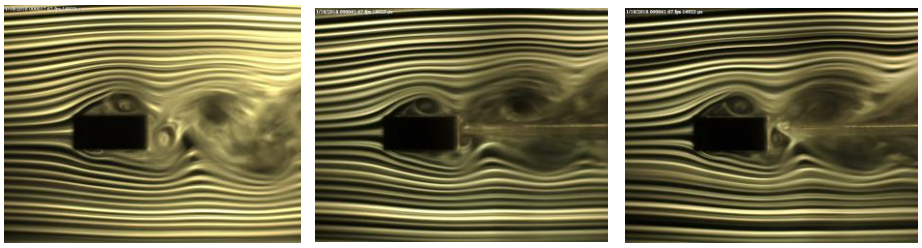

(a)without S.P. (b) with S.P. of g=0.10B (c) with S.P. of g=0.25B

Fig. 5 Flow visualization test results of forced-oscillating model of B/D=2.0 at the bottom displacement in $2\eta/D$=0.20 at Vr=5.45

3.2 B/D=4.0 Rectangular Cross Section

The result of the spring-supported test of the case of B/D = 4.0 is shown in Fig. 6. The vortex-induced vibrations occurring at roughly Vr = 3 and Vr = 7 were confirmed. They are considered to be motion-induced vortex vibrations because these vortex-induced vibrations were occurring at $V_{cr,n=2}$=(1/n)1.67×B/D=(1/2)1.67×4.0= 3.33 and $V_{cr,n=1}$=(1/n)1.67×B/D=1.67×4.0=6.67, and there was no change in onset reduced wind speed when S.P. was installed. The result obtained was that when S.P. was installed at g = 0.10B, the response decreased. This result corresponds to those of previous research of Matsumoto et al. (2008). Meanwhile, the result obtained was that when S.P. was installed at g = 0.31B, the response increased. This result also corresponds to the results of previous research of Matsumoto et al. (1993b).

The results of the flow visualization experiment under the condition that reduced wind speeds were Vr = 4.29 and Vr = 8.31, where response becomes the maximum, and the forced-oscillating heaving amplitude was set as $2\eta/D$ = 0.2 were compared with the results of three cases where no S.P. was installed and cases where it was installed at g = 0.10B or g =0.31B. The results are shown in Fig. 7 and Fig. 8, respectively. In either case of reduced wind speed of Vr = 4.29 or Vr = 8.31, when no S.P. was installed, it can be confirmed that the secondary vortex at the trailing edge generated almost constantly separating from the trailing edge. From the fact that when S.P. was installed at g = 0.10B, the generation of the integrated vortex of the separated vortex from the leading edge with the secondary vortex at the trailing edge was inhibited by S.P., it is supposed that the exciting force acting on the model decreased and as a result, the response of motion-induced vortex vibration decreased. It was confirmed when S.P. was installed at g = 0.31B, the integrated vortex can enter the gap strongly between S.P. and the model. In other words, it is considered that the Kármán vortex was not only weakened by the installation of S.P. and separated vortices from leading edge were elicited, but the entrainment of the integrated vortex into the gap between the model and S.P. had a tendency to become strong. As the result, the exciting force acting on the model became large, and the response also became large.

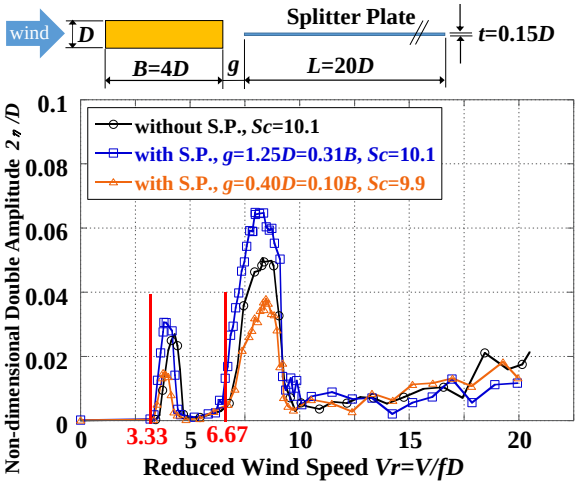

Fig. 6 Spring-supported test result of *B*/*D*=4.0

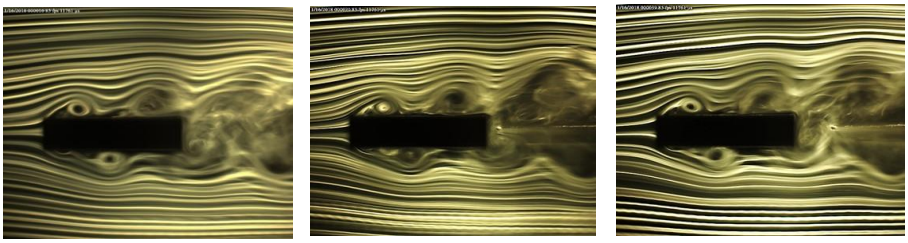

(a)without S.P. (b) with S.P. of g=0.10B (c) with S.P. of g= 0.31B

Fig. 7 Flow visualization test results of forced-oscillating model of *B*/*D*=4.0 at the bottom displacement in $2\eta/D$=0.20 at *Vr*=4.29

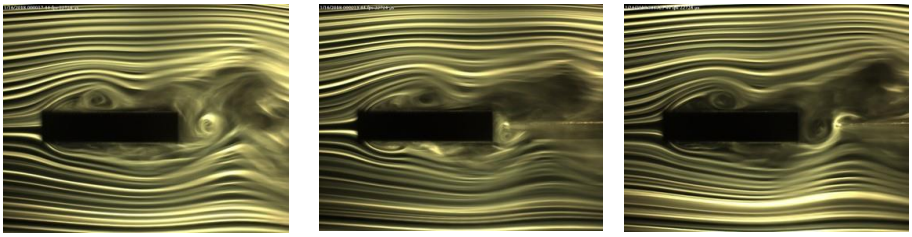

(a)without S.P. (b) with S.P. of g=0.10B (c) with S.P. of g=0.31B

Fig. 8 Flow visualization test results of forced-oscillating model of *B*/*D*=4.0 at the bottom displacement in $2\eta/D$=0.20 at *Vr*=8.31

3.3 B/D=6.0 Rectangular Cross Section

The result of the spring-supported test in the case of B/D = 6 is shown in Fig. 9. The vortex-induced vibrations occurring from approximately Vr = 5 were confirmed. These vortex-induced vibrations are considered to be motion-induced vortex vibrations because they were occurring at $V_{cr,n=2}=(1/n)1.67\times B/D=(1/2)1.67\times 6.0=5.0$ and there was no change in onset reduced wind speed when S.P. was installed. The result was obtained that although the case was the same as that of B/D = 4.0, when S.P. was installed at g = 0.10B, the response of motion-induced vortex vibration decreased; however, the response increased when S.P. was installed at g = 0.33B. Meanwhile, motion-induced vortex vibration was not confirmed, which is considered to occur from approximately $V_{cr,n=1}=(1/n)1.67\times B/D=(1/1)1.67\times B/D=1.67\times 6.0=10.0$.

The result of the experiment of flow visualization under the condition that reduced wind speed was Vr =5.38, where response amplitude becomes the maximum, and the forced-oscillating heaving amplitude was set as $2\eta/D$=0.2 was compared with the results of three cases when no S.P. was installed and cases where it was installed at g = 0.10B and g = 0.33B. The results are shown in Fig. 10. It can be seen that the generation patterns of secondary vortex at trailing edge in all three cases have the same tendency as those in the case of B/D = 4.0. Therefore, it is considered that the response of motion-induced vortex decreased when S.P. was installed at g = 0.10B and it increased when S. P. was installed at g = 0.33B, compared with the response without S.P., just as the same as in the case of B/D = 4.0.

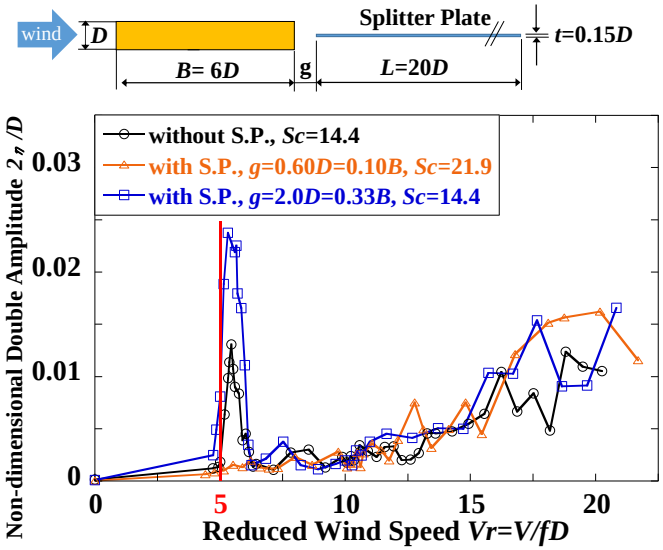

Fig. 9 Spring-supported test result of B/D=6.0

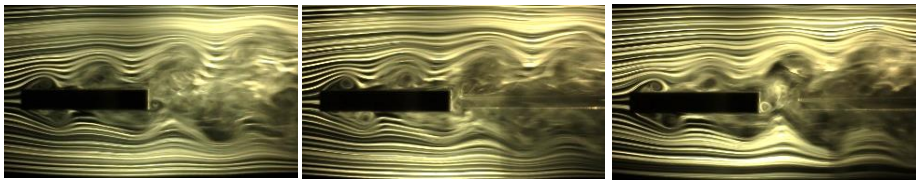

(a)without S.P. (b) with S.P. of g=0.10B (c) with S.P. of g=0.33B

Fig. 10 Flow visualization test results of forced-oscillating model of B/D=6.0 at the bottom displacement in $2\eta/D$=0.20 at Vr=5.38

3.4 Generation probability for secondary vortex at the trailing edge

When the model is photographed for 10 cycles while it is forced-oscillated at reduced wind speed $V_{cr,n=2}$=(1/n)1.67×B/D=(1/2)1.67×B/D=0.83×B/D or $V_{cr,n=1}$=(1/n)1.67×B/D=(1/1)1.67×B/D=1.67×B/D, 20 secondary vortices at the trailing edge are generated at maximum. The generation probability was defined as (the number of generation times/20) ×100 (%), and it was used as an index showing the ratio of contribution of secondary vortex at trailing edge to motion-induced vortex vibration. The results are shown in Fig. 11. The generation probability of the secondary vortices at the trailing edge tends to become higher as the forced-oscillating heaving amplitude $2\eta/D$ increases as the same as the case of B/D=0.62-1.50 shown in Fig. 12 of Matsuda et al. (2017). However, the forced-oscillating amplitude becomes larger for the generation probability to reach 100% in the case of B/D=4.0 and 6.0 at $V_{cr,n=1}$=(1/n)1.67×B/D=1.67× B/D than that in the case of $B/D \leqq 2.0$. This cause is considered to be the interference between motion-induced vortices and Kármán vortices due to the fact that the onset reduced wind speeds of motion-induced vortex vibration and Kármán vortex-induced vibration come close to each other on the cross section at roughly B/D = 2.8-6.0. As a result of the comparisons of Fig. 11 with Fig. 4, Fig. 6 and Fig. 9, which are the results of spring-supported tests of the rectangular cross sections of B/D = 2.0, 4.0 and 6.0, respectively, motion-induced vortex vibration is occurring with the amplitudes smaller than the forced-oscillating amplitude with which the secondary vortex at the trailing edge can fully generate; therefore, it is considered that the secondary vortex at trailing edge does not fully contribute to the onset of motion-induced vortex vibration. Therefore, it is suggested that the secondary vortex at the trailing edge is not always necessary for the onset of motion-induced vortex vibration of the rectangular cross sections of B/D = 2, 4 and 6, as the same as the case of cross section of B/D=0.62-1.50, which are the results of previous research of Matsuda et al. (2017) .

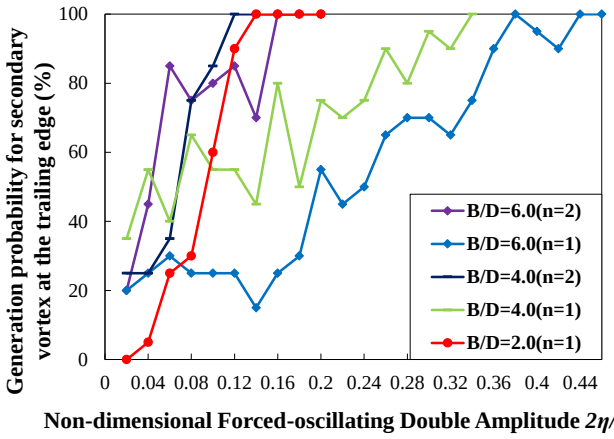

Fig. 11 Generation probability for secondary vortex at the trailing edge (*B/D*=2.0, 4.0, 6.0)

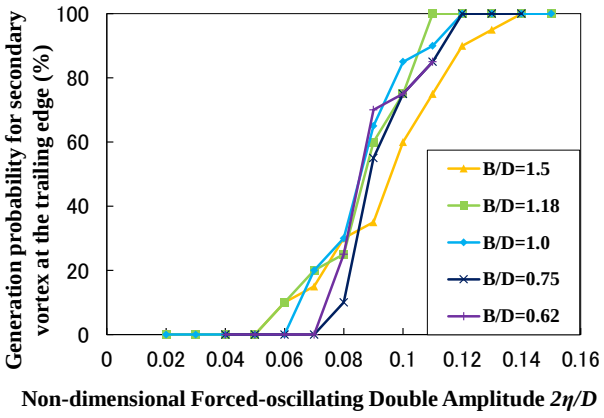

Fig. 12 Generation probability for secondary vortex at the trailing edge (*B/D*=0.62-1.5) (Matsuda et al., 2017)

4 Conclusions

Smoke flow visualizations and spring-supported tests were performed for side ratios of *B/D*=2.0, 4.0, 6.0 in order to elucidate the role of secondary vortices at the trailing edge in motion-induced vortex vibration. The findings obtained from this research are as follows:

1. The secondary vortex at the trailing edge is not always necessary for the onset of motion-induced vortex vibration in heaving motion with *B/D* = 2.0, 4.0 and 6.0 as the same as the results of our previous research targeting of rectangular cross section with the side ratio of *B/D* = 0.62-1.50.
2. It was suggested that the extent of the exciting force of motion-induced vortex vibration in heaving motion of the cross section with the side ratio of *B/D* = 2.0, 4.0 and 6.0 is dependent on the existence of a secondary vortex at the trailing edge.

References

Komatsu, S., and Kobayashi, H. (1980). Vortex-induced oscillation of bluff cylinders, *Journal of Wind Engineering and Industrial Aerodynamics*, 6, 335-362.

Matsuda, K., Kato, Tamai, Y., Suda, K. (2016). Experimental study on aerodynamic vibrations of rectangular cross sections having low side ratios, *Proceedings of 8th International Colloquium on Bluff Body Aerodynamics and Applications*, Northeastern University, Boston, Massachusetts, USA.

Matsuda, K., Kato, K., Arise, K., and Ishii, H. (2017). Study on the Relation between Side Ratios of Rectangular Cross Sections and Secondary Vortices at Trailing Edge in Motion-induced Vortex Vibration, *Proceedings of the ASME 2017 Pressure Vessels & Piping Division Conference*, PVP2017, 65565.

Matsumoto, M., Shiraishi, N., Shirato, H., Stoyanoff, S. and Yagi, T. (1993a). Mechanism of, and turbulence effect on vortex-induced oscillations for bridge box girders, *Journal of Wind Engineering and Industrial Aerodynamics* 49, 1-3, 467-476.

Matsumoto, M., Shiraishi, N., Shirato, H., Yagi, T., Tanaka, M. and Yamagishi, M. (1993b). On mechanism of vortex-induced oscillations for rectangular cylinder, Journal of JSCE Structural Engineering, 39A, 891-896. (in Japanese)

Matsumoto, M., Yagi, T., Tamaki, H. and Tsubota, T. (2008). Vortex-induced vibration and its effect on torsional flutter instability in the case of B/D=4 rectangular cylinder, *Journal of Wind Engineering and Industrial Aerodynamics* 96, 6-7, 971-983.

Nakamura, Y., Ohya, Y., and Tsuruta, H. (1991). Experiments on vortex shedding from flat plates with square leading and trailing edge, *Journal of Fluid Mechanics*, 222, 437-447.

Naudascher, E., and Wang, Y. (1993). Flow-induced vibrations of prismatic bodies and grids of prisms, *Journal of Fluids and Structures*, 7, 341-373.

Novak, M. (1971). Galloping and vortex induced oscillations of structures, *Proceedings of the Third International Conference on Wind Effects on Buildings and Structures*, Tokyo, Japan, 799-809.

Ohya, Y., Nakamura, Y., Ozono, S., Tsuruta, H., and Nakayama, R. (1992). A numerical study of vortex shedding from flat plates with square leading and trailing edges, *Journal of Fluid Mechanics*, 236, 445-460.

Otsuki, Y., Washizu, K., Tomizawa,H., Ohya, A. and Fujii, K. (1971). Experiments on the aeroelastic instability of prismatic bars with rectangular sections, *Proceedings of the Third International Conference on Wind Effects on Buildings and Structures*, Tokyo, Japan, 891-898.

Rockwell, D., and Naudascher, E. (1978). Review- Self-sustaining oscillations of flow past cavities, *Transactions of the ASME, Journal of Fluids Engineering*, 100, 152-165.

Shiraishi, N., and Matsumoto, M. (1983). On classification of vortex-induced oscillation and its application for bridge structures, *Journal of Wind Engineering and Industrial Aerodynamics* 14, 1-3, 419-430.